Journal of Applied Electrochemistry (2022) 52:1607–1616
https://doi.org/10.1007/s10800-022-01731-9

RESEARCH ARTICLE

Facile synthesis of Co_3O_4/C porous polyhedrons for voltammetric determination of quercetin in human serum and urine

Yi Zhang[1] · Liwen Zhang[2] · Tingcui Gong[1] · Tianhao Li[2] · Xuenuan Li[2] · Jun Feng[1,2] · Tingfan Tang[2] · Hao Cheng[2,3]

Received: 19 February 2022 / Accepted: 20 June 2022 / Published online: 20 July 2022

Abstract

Due to the highly porous structure, metal organic framework (MOF)-derived materials are extensively applied in the field of electroanalysis. In this experiment, an effective electrochemical sensing based on Co_3O_4/C-derived ZIF-67 MOF had been constructed for ultrasensitive determination of quercetin at trace level. The resultant Co_3O_4/C porous polyhedron of morphology and nanostructure were carefully examined using transmission electron microscopy (TEM), scanning electron microscopy (SEM), X-ray powder diffraction (XRD), X-ray photoelectron spectroscopy (XPS), and Brunauer–Emmett–Teller (BET) techniques. Differential pulse anodic stripping voltammetry (DPV) method was adopted to analyze quercetin under the optimized conditions. The DPV response of Co_3O_4/C film-coated glass carbon electrode (Co_3O_4/C/GCE) for quercetin determination was achieved a long linearity ranging from 0.5 to 30 μM, achieving high sensitivity about 1.830×10^{-6} A cm^{-2} μM^{-1}, and the detection limit was calculated to be 0.022 μM (S/N = 3). Besides, the fabricated Co_3O_4/C/GCE displayed excellent selectivity, desirable repeatability, and good reproducibility. More importantly, the proposed sensor exhibited satisfactory recovery ranges and accuracy for the determination of trace quercetin in human urine and serum samples, which will make it as an alternative advantageous choice for practical on-site determination.

Graphical abstract

The porous Co_3O_4/C polyhedron derived by ZIF-67 MOF was successfully synthesized.The as-synthesized material was employed to prepare chemically modified electrodefor ultrasensitive determination of quercetin. Then the Co_3O_4/C-modified glass carbon electrode is displayed good sensitivity and accuracy toward quercetin in urine andserum samples.

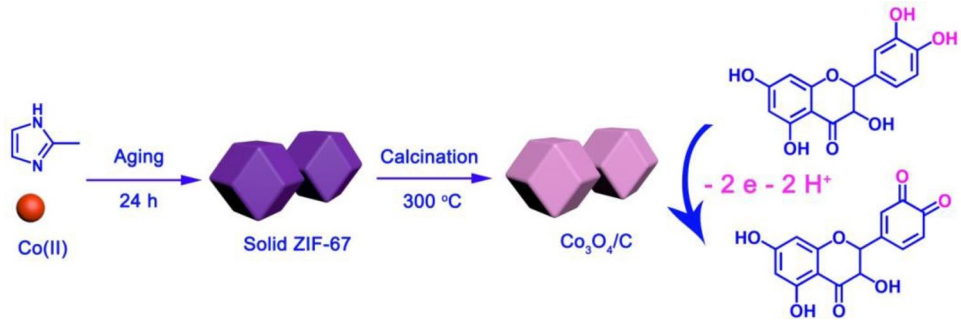

Keywords Co_3O_4/C porous polyhedrons · ZIF-67 template · DPV · Quercetin · Sensor

1 Introduction

Quercetin (3,3′,4′,5,7-penta-hydroxy-flavon, $C_{15}H_{10}O_7$) is a kind of bioactive flavonoid substances and commonly distributes in vegetables, leaves, grains, and fruits [1, 2]. Many researchers have confirmed that quercetin possesses

Yi Zhang and Liwen Zhang have contributed equally to this work.

✉ Hao Cheng
chenghao@gxust.edu.cn

Extended author information available on the last page of the article

a broad range of physiological effects, for example, antioxidant, anti-inflammatory, antiviral, and antitumor properties [3, 4]. Since quercetin is not produced in human body, the safe dose is reported as 945 mg m^{-3} [5]. High doses of quercetin can cause inflammation, DNA structure damage, and hypertension [6]. Eventually, it is significant to design a quick and accurate method for identifying and quantifying of quercetin concentration in biochemistry, clinical medicine, and natural pharmaceutical chemistry samples.

Up to present, many conventional analytical techniques have been established to detect quercetin, for example, high-performance liquid chromatography-mass spectrum (HPLC-MS) [7], UV–Vis spectroscopy [8], capillary electrophoresis, chemiluminescence [9], molecularly imprinted polymer methods [10], etc. But some of these techniques require high price of instruments, time-consuming experimental process, and skilled technicians to carry out the measurements [11–14]. Thus, it is critically important to develop a novel method for the determination of trace amount of quercetin. In contrast to the these traditional laboratory-based analytical techniques, electrochemical technique often offers a cost-effective, simple, easy-to-handle, and sensitive analytical strategy for quercetin determination [15, 16]. Besides, it is worth mentioning that quercetin contains five electro-active hydroxyl groups in its molecular structure [17, 18]. Consequently, electrochemical technique is suitable for fast and in situ determination of quercetin.

Electrochemical approach is generally equipped with an effective working electrode, which is anchored by different nanostructure materials including precious metals [19, 20], metal oxide nanoparticles [21], conducting polymers [22], and functionalized carbon nanocomposites [23]. Among the favored candidates mentioned above, transition metal oxide/C-based nanomaterials, especially Co-based oxide/carbon (CoO_x/C) composites, were widely adopted as catalysts of non-enzymatic sensor in the electrochemical filed [24]. It is mostly attributed to the highly catalytic performance and excellent electrochemical activity of CoO_x/C composites. As a highly porous Co-based MOF, ZIF-67 has been usually recommended as a good precursor or template for the preparation of CoO_x/C composites. Moreover, ZIF-derived materials can not only maintain the structural diversity and porosity characteristics of ZIF but also effectively enhance their conductivity and stability [25]. In fact, the direct utilization of ZIFs in non-enzymatic sensors is limited for their low inherent electrical conductivity. Therefore, combining ZIFs with highly conductive nanomaterials or transforming ZIFs into derivative materials with good conductivity is expected to further achieve improved electrochemical performance. For example, Elhameh et al. introduced Au shell into ZIF-8@ZIF-67 core to achieve ultrahigh sensitivity and fast response toward nitrite [26]. Moreover, Hu et al. reported ZIF-67-derived Co_3O_4@nitrogen-doped carbon nanotube/amino-functionalized graphene quantum dots composites to construct a new electrochemical sensor for luteolin detection [27].

In this work, Co_3O_4/C porous polyhedrons were prepared by an effective and controllable ZIF-67 MOF calcination strategy to improve the conductivity of ZIF-67. Due to the high porosity, remarkable specific surface area, well-defined active sites, and good electrochemical stability, the proposed Co_3O_4/C/GCE exhibited superior electrochemical performance toward quercetin determination.

2 Experimental parts

2.1 Chemicals and materials

Quercetin ($C_{15}H_{10}O_7$, 97%, Mw = 302.24) and $Co(NO_3)_2 \cdot 6H_2O$ (99%, Mw = 291.03) were provided by Macklin Biochemical Co., Ltd (Shanghai, China). CH_3OH (99.5%, Mw = 32.04), NaH_2PO_4 (99.0%, Mw = 119.98), Na_2HPO_4 (99%, Mw = 141.96), H_3PO_4 (≥ 85 wt% in H_2O, Mw = 98.00), ethanol (95%, Mw = 46.07), and DMF (C_3H_7NO, 99.5%, Mw = 73.09) were purchased from Hangxin Experimental Equipment Co., Ltd (Liuzhou, China). 2-methylimidazole ($C_4H_5N_2$, 98%, Mw = 82.10) was obtained from Aladdin Biochemical Technology Co., Ltd (Shanghai, China). A 0.01 M quercetin stock solution was freshly prepared in absolute ethanol and diluted with water. Phosphate buffer solutions (0.1 M PBS) with different pH (pH = 2.0, 2.5, 3.0, 3.5, and 4.0) were prepared by mixing NaH_2PO_4, Na_2HPO_4, and H_3PO_4, saved as a supporting electrolyte. All the reagents were in AR grade and utilized without any further purification.

2.2 Instrumentation

XRD analysis was measured with on a D8 Advance diffractometer (Brucker). SEM was performed on a Merlin instrument (Zeiss). TEM, high-resolution TEM (HR-TEM), and element mapping were recorded by using a Talos F200X G2 (FEI) microscopy. XPS experiment was conducted on a Thermo esca lab system. BET method was utilized to calculate the specific surface area (Micromeritics, Smart VacPrep). High-performance liquid chromatography (HPLC, Shimadzu, LC-20AT) was applied to test the concentration of quercetin in the samples for comparison. All the electrochemical measurements were acquired from a CHI 760e potentiostat (Chenhua Instruments Co., UAS). A classical three-electrode cell with a Co_3O_4/C/GCE (d = 3 mm) working electrode, a Pt wire counter electrode, and an Ag/AgCl (1 M KCl) reference electrode, were adopted in all electrochemical experiments.

Scheme 1 Schematic description of the synthesis of Co_3O_4/C polyhedron

2.3 Synthesis of Co_3O_4/C polyhedron

ZIF-67 self-sacrificial template was prepared according to a modified method reported in the literature [28]. Typically, 1.312 g 2-methylimidazole and 0.996 g $Co(NO_3)_2{\cdot}6H_2O$ were added into 100 mL CH_3OH. Subsequently, the mixture solution was stirred for 2 h and then aged for 24 h at room temperature. After the reaction, the purple ZIF-67 precipitates were collected from the supernatant solution by centrifugation, washed with a large amount of CH_3OH for several times, and dried overnight at 60 °C in a vacuum. Further, the ZIF-67 precursor was continuously calcined at 300 °C for 2 h under air atmosphere in a tube furnace. After cooling to room temperature, the Co_3O_4/C powder was collected. The overall preparation procedure of Co_3O_4/C polyhedron is shown in Scheme 1.

2.4 Fabrication of the Co_3O_4/C/GCE

Prior to the modification, GCE was carefully polished by Al_2O_3 slurry with the particle size of 0.3 and 0.05 μm Al_2O_3 to form a mirror-like surface. Then, the polished GCE was cleaned successively in water and ethanol to remove surface contamination. The Co_3O_4/C/GCE was fabricated by the following method. First, 3 mg Co_3O_4/C was dispersed and sonicated in 2 mL DMF to make a homogeneous suspension. Subsequently, 5.0 μL of above solution was placed on the freshly surface of GCE. At last, the Co_3O_4/C electrode was allowed to dry completely at room temperature.

2.5 Electrochemical detection of quercetin

The DPV and cyclic voltammogram (CV) for determination of quercetin were performed in PBS (0.1 M, 10 mL). The deposition time is 90 s. DPV and CV potential scan were conducted in the range of 0.1 – 0.7 V vs. Ag/AgCl and 0.05 –0.7 V vs. Ag/AgCl, respectively. All experiments were measured in air at room temperature (25 ± 5 °C).

3 Results and discussion

3.1 Characterizations of products

The morphology of the as-prepared ZIF-67 crystal and Co_3O_4/C composite was investigated by SEM technology. As exhibited in Fig. 1a, the collected ZIF-67 nanoparticles are monodispersed and formed rhombic dodecahedral faces via the precipitation process between Co(II) nodes and 2-methylimidazole ligands in CH_3OH. Figure 1b displays the SEM image of Co_3O_4/C hybrid. Obviously, after a facile-annealing process, the obtained Co_3O_4/C nanocomposite inherits the original polyhedral morphology of the ZIF-8

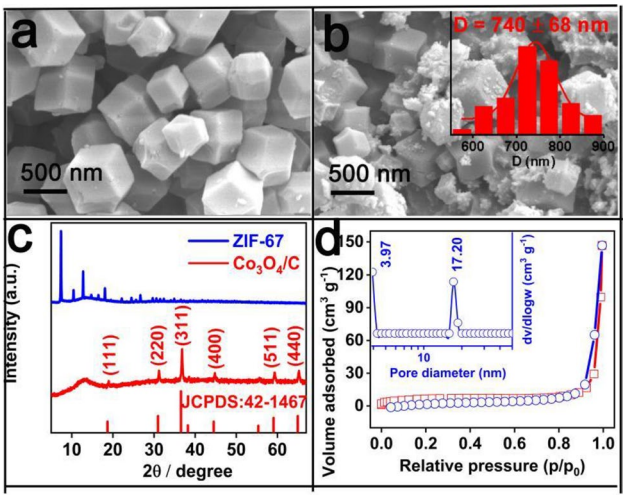

Fig. 1 The SEM images of the as-synthesized **a** ZIF-67 template and **b** Co_3O_4/C hybrid. **c** Powder XRD patterns of the as-prepared ZIF-67 crystal and Co_3O_4/C hybrid. **d** N_2 adsorption–desorption isotherm of porous Co_3O_4/C hybrid and the BJH pore-size distribution plot (inset)

precursor. Some polyhedral structures are collapsed due to the thermal effect. Additionally, the average particle size of Co_3O_4/C composite was estimated to be 740 ± 68 nm (inset of Fig. 1b).

Next, the crystal structure and phase purity of the as-prepared materials were assessed by powder XRD measurement. As observed in Fig. 1c, all of the diffraction peaks of the as-prepared ZIF-67 could be well indexed to those of

ZIF-67 reported in previous work, demonstrating the successful preparation of pure ZIF-67 crystal [29]. After calcination at high temperature, six new diffraction peaks at 19.0°, 31.3°, 36.8°, 44.8°, 59.3°, and 65.2° were observed and attributed to the (111), (220), (311), (400), (511), and (440) reflection planes of Co_3O_4 phase (JCPDS, card No. 42-1467), respectively. The observed pattern is matched well with the standard data of Co_3O_4, and no other impure peaks than Co_3O_4 are observed, suggesting that ZIF-67 templates have been successfully converted into Co_3O_4 by pyrolysis.

The surface area and pore texture of Co_3O_4/C polyhedron were also analyzed as represented in Fig. 1d. The N_2 adsorption/desorption curve likely belongs to the IV type isotherm with a small hysteresis loop according to IUPAC classification, which indicates the coexistence of pore and mesopore in Co_3O_4/C hybrid. The BET-specific surface area of the synthesized of Co_3O_4/C is found to be 24 m^2 g^{-1}. The corresponding BJH pore-size distribution curve is given in the inset of Fig. 1d. It reveals that Co_3O_4/C is mainly mesoporous structure and the pore diameters are 3.97 and 17.20 nm. A relatively specific surface area and abundant porous structure of the as-prepared samples are conducive to electrolyte access and analytes diffusion to active sites, leading to high sensitivity toward quercetin determination.

In general, TEM and HR-TEM analysis were used to characterize the nanostructure of the synthetic Co_3O_4/C particles. When the ZIF-67 precursor was calcined at 300 °C in air atmosphere, ZIF-67 precursor was burned out, releasing CO_2, H_2O, NO_x, and other gases. Ultimately, the ligands in ZIF-67 precursor converted into conductive carbon skeleton and the Co(II) was further transformed into Co_3O_4 particles. As illustrated in Fig. 2a, the overall morphology of the Co_3O_4/C nanoparticle is similar to that of pristine ZIF-67 crystal, with dodecahedron structure. Meanwhile, the surface of Co_3O_4/C particle shows obvious transparent, porous, and fluffy microstructure. Interestingly, the HR-TEM image of Co_3O_4/C sample clearly reveals two sets of lattice fringes with interplanar distances of 0.47 and 0.28 nm, consisted with the (111) and (220) lattice planes of Co_3O_4, respectively (Fig. 2b). Elemental mapping analysis of the Co_3O_4/C polyhedron was also investigated. As displayed in Fig. 2c-h, Co, O, N, and C elements are almost uniformly distributed on the Co_3O_4/C composite. It indicates that ZIF-67 could be a good candidate for the synthesis of the fine-dispersed cobalt-based catalyst.

Then XPS analysis was performed to check the chemical state as well as the elemental composition of the Co_3O_4/C surface. The full XPS spectra of Co_3O_4/C nanocomposite demonstrate the presence of C, N, O, and Co elements (Fig. 3a) and the corresponding element contents are 51.26, 0.93, 34.68, and 12.78 wt%, respectively (Fig. 3b). The high-resolution Co2p is shown in Fig. 3c. The spectrum in the Co2p region exhibits $Co2p_{3/2}$ (780.4 eV) and $Co2p_{1/2}$

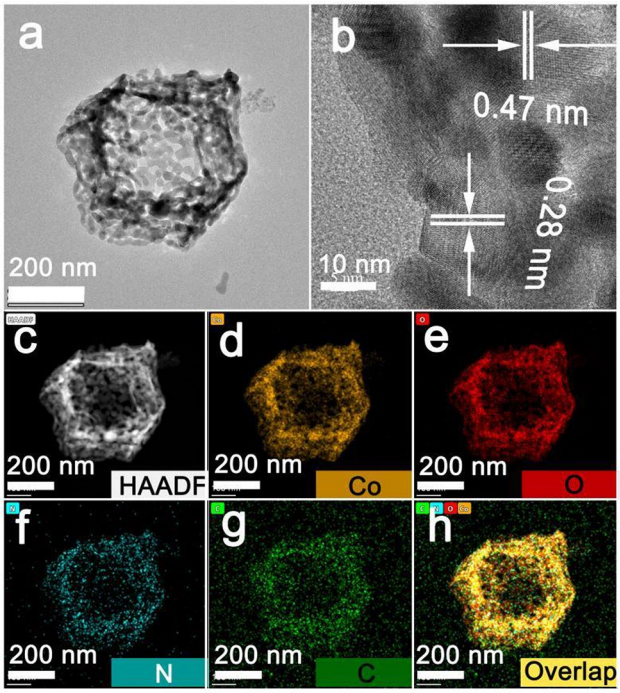

Fig. 2 **a** TEM, **b** HR-TEM, and **c** HADDF images of Co_3O_4/C hybrid. The corresponding EDX mapping of **d** Co, **e** O, **f** N, **g** C, and **h** overlap elements acquired at the same position of Co_3O_4/C material

(795.6 eV) spin orbits of Co_3O_4 phase, respectively [30], which further verifies the formation of Co_3O_4 on the surface of nanocomposite. Moreover, two shakeup satellite peaks are also found at 787.7 and 803.7 eV, respectively. By deconvoluting the XPS spectrum of Co2p, the binding energies at 797.3 eV ($Co2p_{1/2}$) and 781.7 eV ($Co2p_{3/2}$) are assigned to the Co(II) chemical state and the fitted peaks at 795.0 eV ($Co2p_{1/2}$) and 779.8 eV ($Co2p_{3/2}$) can be attributed to Co(III) chemical state [31]. Figure 3d depicts the high-resolution scan of O1s spectra. The characteristic peaks of O – Co(III)/Co(II), HO – C = O, and C = O are located at 530.2, 531.7, and 533.2 eV, respectively [32]. Also, the high-resolution N1s spectrum (Fig. 3e) is well fitted into three small peaks located at 398.4, 399.1, and 400.4 eV, correlating to pyridinic N, pyrrolic N, and graphitic N, respectively [33]. Two types of carbon functional groups are identified in material (Fig. 3f) and the characteristic peaks occupied at 284.5 and 285.3 eV are ascribed to C – C and C – N bond, respectively [34].

3.2 Optimization of conditions

To achieve ultrasensitive and fast determination of trace level of quercetin at Co_3O_4/C/GCE, the concentrations of Co_3O_4/C and deposition time were carefully optimized.

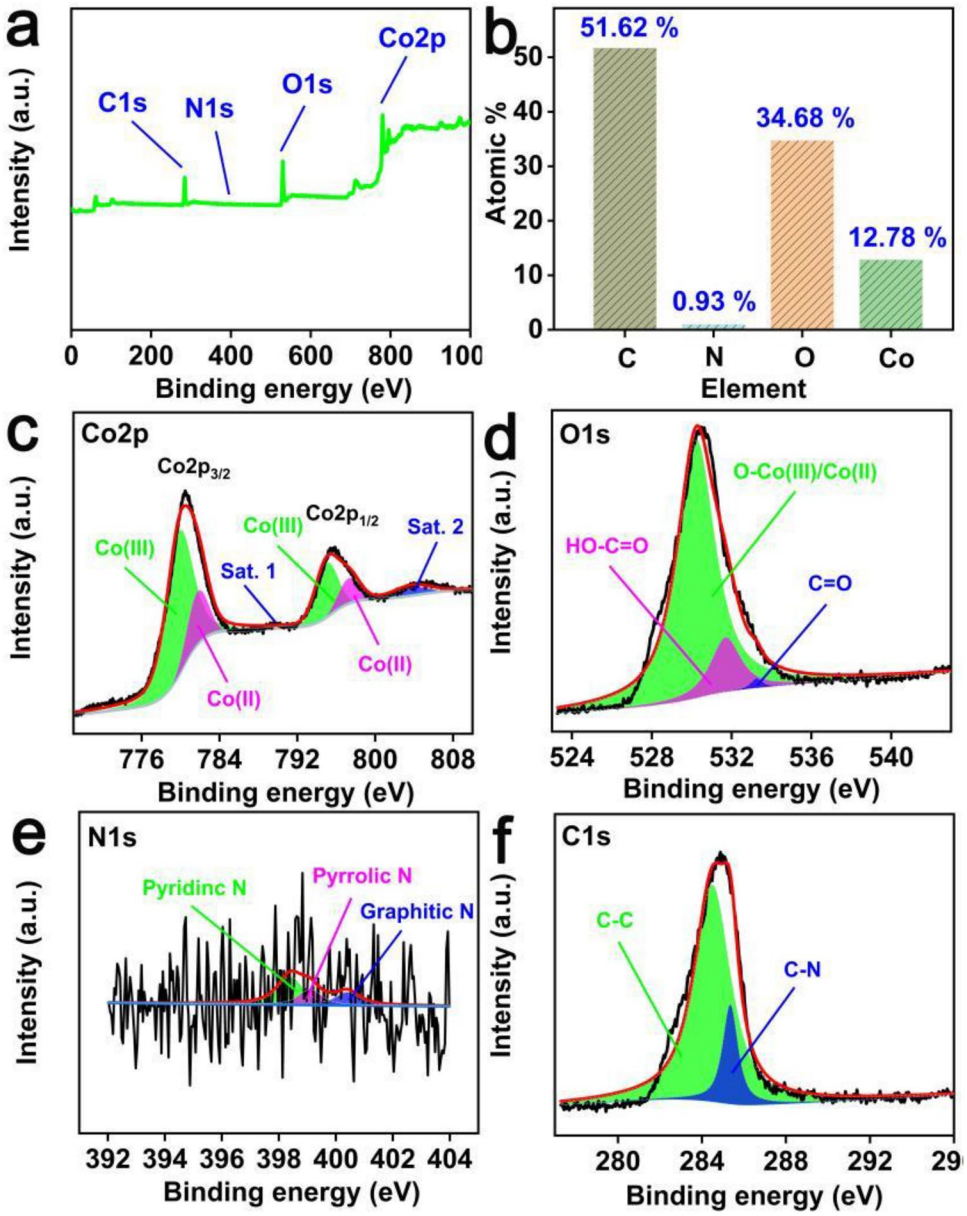

Fig. 3 **a** XPS survey spectra of Co_3O_4/C nanocomposite. **b** The corresponding element content of XPS survey spectra. High-resolution XPS spectrum of Co_3O_4/C nanocomposite: **c** Co2p, **d** O1s, **e** N1s, and **f** C1s

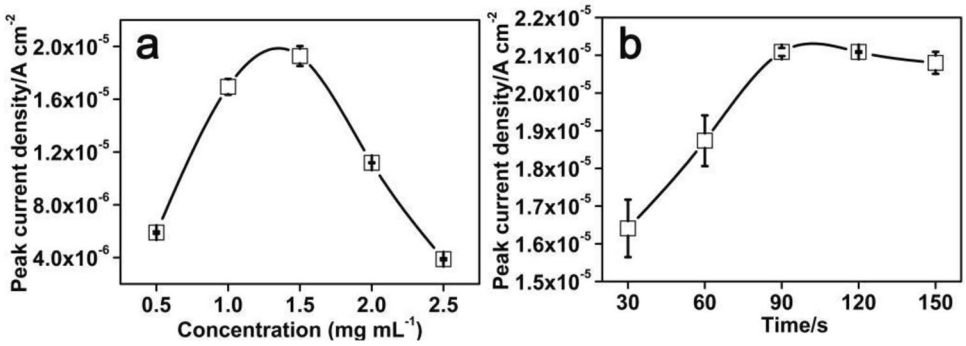

Fig. 4 The effects of **a** Co_3O_4/C concentration and **b** deposition time on the voltammetric responses of 10 μM quercetin in 0.1 M PBS. ($n = 3$)

The influence of the concentration of Co_3O_4/C on the DPV response of detecting quercetin was studied. As can be seen from Fig. 4a, when the concentration of Co_3O_4/C increases from 0.5 to 1.5 mg mL^{-1}, the peak current of DPV increases sharply. Nevertheless, the signal declines notably with Co_3O_4/C concentration above 1.5 mg mL^{-1}. It

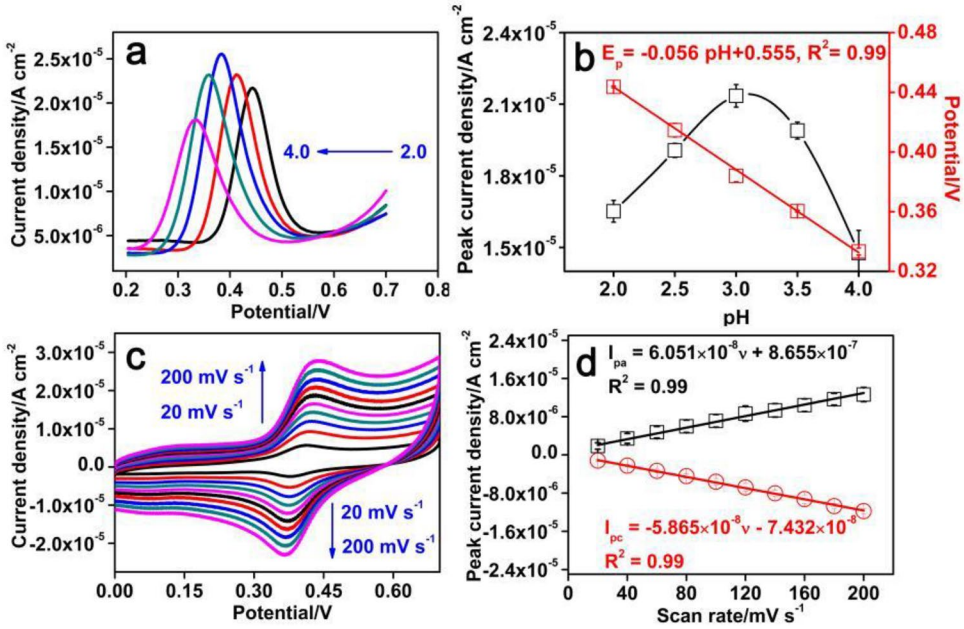

Fig. 5 **a** The influence of pH on the DPV peak current of 10 μM quercetin at Co_3O_4/C/GCE and **b** the corresponding relationships of the I_p-pH and E_p-pH, respectively ($n = 3$). **c** CV curves of 10 μM quercetin on Co_3O_4/C/GCE with different scanning rates between 20 and 200 mV s^{-1} in 0.1 M PBS (pH = 3.0) and **d** the corresponding linear relationships of the $I_{p.a.}$ and I_{pc} vs. υ

is because the thick Co_3O_4/C film can restrict the electron transferred from quercetin to the surface of GCE [35]. Thus, 1.5 mg mL^{-1} of Co_3O_4/C hybrid was chosen to construct sensor.

Meanwhile, the effect of deposition time on oxidation peak currents was examined. As illustrated in Fig. 4b, the oxidation peak current of Co_3O_4/C/GCE rises sharply by increasing of deposition time from 0 to 90 s and appears a platform with the further extension of deposition time. It confirmed that the accumulated saturation could be completed within about 90 s [36]. Consequently, we selected 90 s as optimal deposition time for quercetin detection.

3.3 Electrochemical properties of Co_3O_4/C/GCE

The process of mass transport between the surface of Co_3O_4/C/GCE and the supporting electrolyte is related to the pH of electrolyte. Thus, the influence of the pH value varied from 2.0 to 4.0 on the Co_3O_4/C/GCE was explored by DPV. As illustrated in Fig. 5a, with the increase of pH value, the oxidation peak potential shifts negatively. The result confirms that protons are directly took part in the electrode reaction of quercetin. Furthermore, the corresponding current responses in different pHs are shown in Fig. 5a (black curve). It can be obtained that the DPV signal reaches a maximum value at pH 3.0. So, the pH value of electrolyte is chosen as 3.0 for electrochemical detection of quercetin.

In addition, the variations of oxidation peak potential (E_p) for quercetin are linearly with the changes of pH value, and the regression equation could be calculated as follows: $E_p(V) = -0.056\ \mathrm{pH} + 0.555$, $R^2 = 0.999$ (red line in Fig. 5b). The slope value of above equation is -56 mV pH^{-1}, which is close to the theoretical value -59 mV pH^{-1} in the Nernst equation [37], implying that the ratio of electron and proton number involving in the electrocatalytic redox process is 1:1 [38].

On the Co_3O_4/C/GCE, the average separation of oxidation potential ($_{\Delta}$Ep) in Fig. 5a is about 34 mV, based on the formula of 2.3 RT/nF [39], the electron transfer number of n can be estimated to be 1.64, implying that two electron and two proton transfers take part in the quasi-reversible redox reaction of quercetin at Co_3O_4/C/GCE.

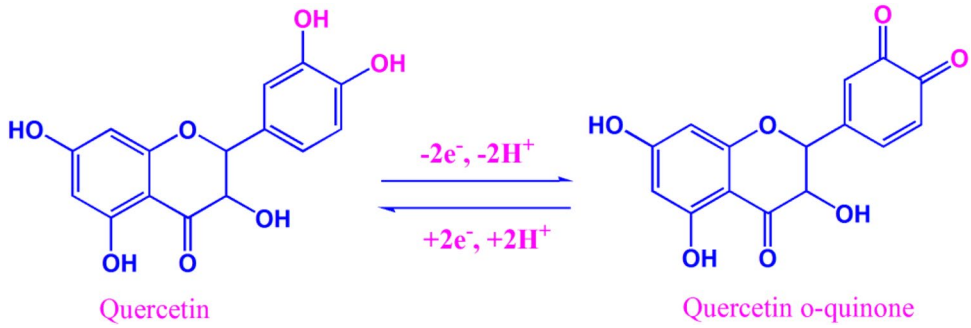

Scheme 2 The reaction mechanism of quercetin on Co_3O_4/C/GCE

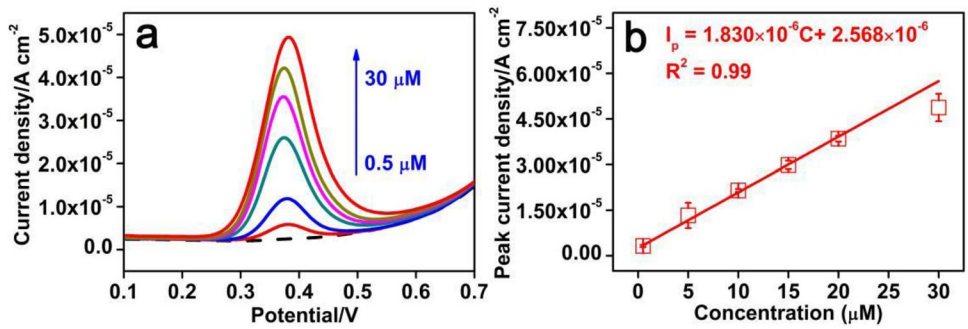

Fig. 6 **a** DPV curves of quercetin detection (C = 0, 0.5, 5, 10, 15, 20, 25, and 30 μM) in PBS solution using the Co_3O_4/C/GCE and **b** the corresponding calibration plot between I_p and C

The electrochemical reaction mechanism of quercetin on the fabricated electrode could be described as Scheme 2.

The electrochemical kinetics of the reaction can be perceived from the scan rate measurement. Hence, the electrochemical efficiency of prepared Co_3O_4/C/GCE in 10 μM quercetin was examined with different scanning rates (υ = 20, 40, 60, 80, 100, 120, 140, 160, 180, and 200 mV s^{-1}). As displayed in Fig. 5c, with increasing of the scan rate (υ), the anodic and cathodic peak currents ($I_{p.a.}$ and I_{pc}) of quercetin concentration enhance simultaneously, accompanied with an enlargement of the peak separation. Moreover, both $I_{p.a.}$ and I_{pc} are increased proportionally with υ, which reveals that the electrochemical reaction is quasi-reversible. And the corresponding linear regression equations are $I_{p.a.}$ (A cm^{-2}) = 6.051×10^{-8} υ (mV s^{-1}) + 8.655×10^{-7} and $R^2 = 0.99$ and I_{pc} (A cm^{-2}) = -5.865×10^{-8} υ (mV s^{-1}) − 7.432×10^{-8}, $R^2 = 0.99$, respectively. All the results demonstrate that quercetin oxidation on Co_3O_4/C/GCE is an adsorption-controlled process [40].

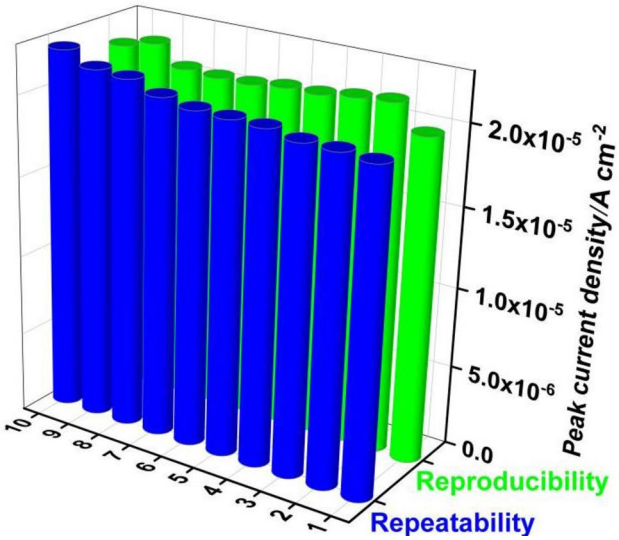

Fig. 7 Repeatability DPV response of sensor with the same Co_3O_4/C/GCE and reproducibility DPV response of senor for ten different Co_3O_4/C/GCEs for determination of 10 μM quercetin under optimal conditions

3.4 Determination of quercetin

The determination of quercetin was performed on Co_3O_4/C/GCE by DPV method, under the optimal experimental conditions: concentration of Co_3O_4/C nanocomposite 1.5 mg mL^{-1}; deposition time 90 s; pH 3.0. Figure 6a shows the DPV responses for quercetin at the concentration ranging from 0.5 to 30 μM. The well-defined peaks of quercetin are observed clearly at the Co_3O_4/C/GCE, and the corresponding peak potentials are found at approximately 0.38 V. Figure 6b displays that the corresponding stripping peak current was plotted against the concentration of quercetin. The linear regression equation for quercetin is presented as follows: I_p (A cm^{-2}) = 1.830×10^{-6} C (μM) + 2.568×10^{-6}, in a linear dynamic response from 0.5 to 30 μM, with the correlation coefficient of $R^2 = 0.99$. On the other hand, the low detection

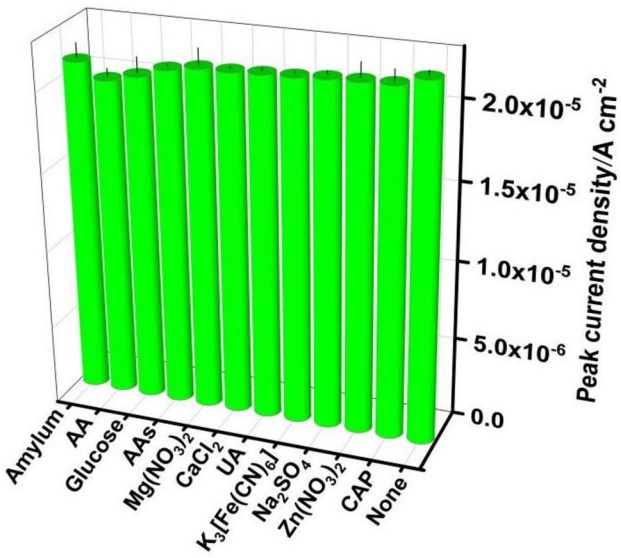

Fig. 8 Interference study performed in 0.1 M PBS with 10 μM quercetin in the absence and presence of 500 μM interfering substances using Co_3O_4/C/GCE under optimal conditions. ($n = 3$)

limit (LOD, S/N = 3) about 0.022 μM and a good sensitivity of 1.830×10^{-6} A cm^{-2} μM^{-1} are obtained for the voltammetric measurements of quercetin. The analytical properties obtained on Co_3O_4/C/GCE reveal that our preparation strategy shows a low LOD and wide linear relationship.

3.5 Repeatability, reproducibility and selectivity

To access the repeatability of the constructed sensor, ten consecutive measurements were performed with the same Co_3O_4/C/GCE to determination 10 μM quercetin, and the mean peak current is $2.089 \times 10^{-5} \pm 8.043 \times 10^{-7}$ A cm^{-2} and the relative standard deviation (RSD) is calculated to be 3.85%. Furthermore, the reproducibility of the modified electrode was also investigated. Ten different Co_3O_4/C/GCEs were verified using the DPV response of 10 μM quercetin. The mean peak current of $2.107 \times 10^{-5} \pm 5.525 \times 10^{-7}$ A cm^{-2} and RSD of 2.62% are obtained, respectively. These attained RSDs are less than 5%, implying a significantly low deviation with excellent fabrication repeatability and reproducibility.

Furthermore, to check the possible interfering species, a selectivity test was carried out by adding different interferences, such as chloramphenicol (CAP), $Zn(NO_3)_2$, Na_2SO_4, $K_3[Fe(CN)_6]$, uric acid (UA), $CaCl_2$, $Mg(NO_3)_2$, aristolochic acids (AAs), glucose, ascorbic acid (AA), and amylum at a 50-fold concentration. The analysis results are given in Fig. 8. No remarkable interferences are found in the DPV signal for all evaluated species. These data imply that Co_3O_4/C-based sensor could be used in the practical application of quercetin with outstanding selectivity.

3.6 Analysis of urine and serum samples

In order to accurately evaluate the validity of proposed method for monitoring of quercetin in real samples, the Co_3O_4/C/GCE was employed to analyze the concentration of quercetin in human urine and blood serum samples. All samples were provided by the second affiliated hospital of Guangxi University of Science and Technology. The standard addition method was utilized to the analysis of quercetin in all samples. The urine and blood serum samples were spiked with standard quercetin solution with concentrations of 0, 2, 10, and 20 μM, respectively. The consequence of recovery experiment acquired in this work is summarized in Table 1. As indicated by the result, the developed sensor has good recoveries, and the RSDs of the modified electrode are less than 5%. Moreover, the results are in good agreement with that of HPLC. The obtained results demonstrate that the recovery rates are accuracy and reliability, indicating that the fabricated sensor used in clinical testing have been confirmed. Detection of quercetin in human urine and serum samples by using

Table 1 Detection of quercetin in human urine and serum samples by Co_3O_4/C/GCE and HPLC. (n = 3)

Samples	Added (μM)	Found ± SD by DPV[a] (μM)	Recovery (%)	RSD (%)	HPLC (μM)
Urine	0	–	–	–	0.00
	2	1.93±0.10	96.42	4.89	1.99
	10	10.04±0.50	100.36	4.95	9.62
	20	19.87±0.21	99.34	1.06	19.87
Serum	0	–	–	–	0.00
	2	1.95±0.09	97.70	4.49	1.99
	10	10.20±0.12	101.96	1.22	10.38
	20	19.96±0.43	99.78	2.13	19.46

[a]Mean value ± standard deviation (SD)

4 Conclusion

In conclusion, a ZIF-67 template-assisted Co_3O_4/C-based electrochemical sensor was fabricated for the determination of quercetin. The unique pore structure of Co_3O_4/C polyhedron provides a large amount of attachment sites for quercetin molecules, as well as the presence of conductive carbon of in the hybrid can effectively electron transfer rate. The Co_3O_4/C/GCE exhibits excellent detection limit, high reproducibility, repeatability, and anti-interference. Moreover, taking real samples of human urine and serum, Co_3O_4/C/GCE proves satisfactory results for quercetin detection from these samples. The present work suggests that Co_3O_4/C sensor is a potential candidate for the determination of clinical samples, which will a promising cost-effective approach in electrochemical analysis.

Acknowledgements This work was supported by the State Key Laboratory for Chemistry and Molecular Engineering of Medicinal Resources (Guangxi Normal University) (CMEMR2019-B10) and Light of Bagui of Academic Research and Studies Program in 2021 (Gui Zu Tong Zi, Document No. 64 of 2021).

Declarations

Conflict of interest There is no conflict of interest in this paper.

References

1. Nghia NN, Huy BT, Lee YI (2020) Highly sensitive and selective optosensing of quercetin based on novel complexation with yttrium ions. Analyst 145:3376–3384
2. Chen Y, Huang W, Chen K, Zhang T, Wang Y, Wang J (2019) Facile fabrication of electrochemical sensor based on novel core-shell PPy@ZIF-8 structures: enhanced charge collection for quercetin in human plasma samples. Sens Actuators B 290:434–442
3. Saritha D, Koirala AR, Venu M, Reddy GD, Reddy AVB, Sitaram B, Madhavi G, Aruna K (2019) A simple, highly sensitive and stable electrochemical sensor for the detection of quercetin in solution, onion and honey buckwheat using zinc oxide supported on carbon nanosheet (ZnO/CNS/MCPE) modified carbon paste electrode. Electrochim Acta 313:523–531
4. Luo G, Deng Y, Zhu L, Liu J, Zhang B, Zhang Y, Sun W, Li G (2020) Au-Co nanoparticles-embedded N-doped carbon nanotube hollow polyhedron modified electrode for electrochemical determination of quercetin. Mikrochim Acta 187:546
5. Durai L, Kong CY, Badhulika S (2020) One-step solvothermal synthesis of nanoflake-nanorod WS_2 hybrid for non-enzymatic detection of uric acid and quercetin in blood serum. Mater Sci Eng C Mater Biol Appl 107:110217
6. Liu Y, Xie R, Yang P, Lu L, Shen L, Tao J, Liu Z, Zhao P (2020) An excellent electrochemical sensor based on highly porous gold film modified gold electrode for detecting quercetin in food and medicine. J Electrochem Soc 167:047514
7. Rahimi M, Bahar S, Heydari R, Amininasab SM (2019) Determination of quercetin using a molecularly imprinted polymer as solid-phase microextraction sorbent and high-performance liquid chromatography. Microchem J 148:433–441
8. Soylak M, Ozdemir B, Yilmaz E (2020) An environmentally friendly and novel amine-based liquid phase microextraction of quercetin in food samples prior to its determination by UV-vis spectrophotometry. Spectro Acta Part A, Mol Biomol Spectr 243:118806
9. Memon AF, Solangi AR, Memon SQ, Mallah A, Memon N, Memon AA (2016) Simultaneous determination of quercetin, rutin, naringin, and naringenin in different fruits by capillary zone electrophoresis. Food Anal Methods 10:83–91
10. Xu L, Pan M, Fang G, Wang S (2019) Carbon dots embedded metal-organic framework@molecularly imprinted nanoparticles for highly sensitive and selective detection of quercetin. Sens Actuators B 286:321–327
11. Alam AU, Deen MJ (2020) Bisphenol aelectrochemical sensor using graphene oxide and beta-cyclodextrin-functionalized multi-walled carbon nanotubes. Anal Chem 92:5532–5539
12. Mettakoonpitak J, Volckens J, Henry CS (2020) Janus electrochemical paper-based analytical devices for metals detection in aerosol samples. Anal Chem 92:1439–1446
13. Tao H, Zhang S, Chen C (2018) A design of Wsn based locking system. Acta Info Malaysia 2:4–6
14. Gupta JK, Gupta SK (2019) A comparative study of crowd counting and profiling through visual and non-visual sensors. Acta Info Malaysia 3:4–6
15. Hwang JH, Islam MA, Choi H, Ko TJ, Rodriguez KL, Chung HS, Jung Y, Lee WH (2019) Improving electrochemical Pb^{2+} detection using a vertically aligned 2D MoS_2 nanofilm. Anal Chem 91:11770–11777
16. Lakshmanakumar M, Nesakumar N, Kulandaisamy AJ, Rayappan JBB (2021) Principles and recent developments in optical and electrochemical sensing of dopamine: a comprehensive review. Measurement 183:109873
17. Saljooqi A, Shamspur T, Mostafavi A (2020) Fe_3O_4@SiO_2-PANI-Au nanocomposite prepared for electrochemical determination of quercetin in food samples and biological fluids. Electroanalysis 3:1–8
18. Kuyumcu Savan E (2019) Square wave voltammetric (SWV) determination of quercetin in tea samples at a single-walled carbon nanotube (SWCNT) modified glassy carbon electrode (GCE). Anal Lett 53:858–872
19. Ibrahim M, Ibrahim H, Almandil NB, Sayed MA, Kawde AN (2020) A new hybrid nanocomposite electrode based on Au/CeO_2-decorated functionalized glassy carbon microspheres for the voltammetric sensing of quercetin and its interaction with DNA. Anal methods: Adv methods Appl 12:2846–2857
20. Cao M, Chang Z, Tan J, Wang X, Zhang P, Lin S, Liu J, Li A (2022) Superoxide radical-mediated self-synthesized Au/MoO_{3-x} hybrids with enhanced peroxidase-like activity and photothermal effect for anti-MRSA therapy. ACS Appl Mater Interfaces 14:13025–13037
21. Tajyani S, Babaei A (2018) A new sensing platform based on magnetic Fe_3O_4@NiO core/shell nanoparticles modified carbon paste electrode for simultaneous voltammetric determination of quercetin and tryptophan. J Electroanal Chem 808:50–58
22. Karakaya S, Kaya İ (2021) An electrochemical detection platform for selective and sensitive voltammetric determination of quercetin dosage in a food supplement by poly(9-(2-(pyren-1-yl) ethyl)-9 h-carbazole) coated indium tin oxide electrode. Polymer 212:123300
23. Zhao P, Ni M, Xu Y, Wang C, Chen C, Zhang X, Li C, Xie Y, Fei J (2019) A novel ultrasensitive electrochemical quercetin sensor based on MoS_2-carbon nanotube@graphene oxide nanoribbons/HS-cyclodextrin/graphene quantum dots composite film. Sens Actuators B 299:126997

24. Qiu W, Tanaka H, Gao F, Wang Q, Huang M (2019) Synthesis of porous nanododecahedron Co_3O_4/C and its application for nonenzymatic electrochemical detection of nitrite. Adv Powder Technol 30:2083–2093
25. Cui W, Kang X, Zhang X, Zheng Z, Cui X (2019) Facile synthesis of porous cubic microstructure of Co_3O_4 from ZIF-67 pyrolysis and its Au doped structure for enhanced acetone gas-sensing. Phys E 113:165–171
26. Saeb E, Asadpour-Zeynali K (2022) A novel ZIF-8@ZIF-67/Au core-shell metal organic framework nanocomposite as a highly sensitive electrochemical sensor for nitrite determination. Electrochim Acta 417:140278
27. Hu Y, Zhang L, Zhao P, Wang C, Fei J, Xie Y (2022) Ultrasensitive luteolin electrochemical sensor based on zeolitic imidazolate frameworks-derived cobalt trioxide@nitrogen doped carbon nanotube/amino-functionalized graphene quantum dots composites modified glass carbon electrode. Sens Actuators B 351:130938
28. Jo Y-M, Kim T-H, Lee C-S, Lim K, Na CW, Abdel-Hady F, Wazzan AA, Lee J-H (2018) Metal-organic framework-derived hollow hierarchical Co_3O_4 nanocages with tunable size and morphology: ultrasensitive and highly selective detection of methylbenzenes. ACS Appl Mater Interfaces 10:8860–8868
29. Zhang C, Chu W, Jiang R, Li L, Yang Q, Cao Y, Yan J (2019) ZIF-67 derived hollow structured Co_3O_4 nanocatalysts: tunable synthetic strategy induced enhanced catalytic performance. Catal Lett 149:3058–3065
30. Bai L, Guan Z, Li S, Zhang S, Huang Q, Li Z (2021) Nest-like Co_3O_4 and PdO/Co_3O_4 synthesized via metal organic framework with cyclodextrin for catalytic removal of bisphenol A by persulfate. Sep Purif Technol 255:117718
31. Doan TLH, Kim J-Y, Lee J-H, Nguyen LHT, Dang YT, Bui K-BT, Pham ATT, Mirzaei A, Phan TB, Kim SS (2021) Preparation of n-ZnO/p-Co_3O_4 heterojunctions from zeolitic imidazolate frameworks (ZIF-8/ZIF-67) for sensing low ethanol concentrations. Sens Actuators B 348:130684
32. Devi RK, Muthusankar G, Chen S-M, Gopalakrishnan G (2021) In situ formation of Co_3O_4 nanoparticles embedded N-doped porous carbon nanocomposite: a robust material for electrocatalytic detection of anticancer drug flutamide and supercapacitor application. Microchim Acta 188:1–15
33. Bai L, Zhang J, He J, Zheng H, Yang Q (2021) ZnO-Co_3O_4/N-C cage derived from the hollow Zn/Co ZIF for enhanced degradation of bisphenol A with persulfate. Inorg Chem 60:13041–13050
34. Li H, Lu B, Zhang W, Cao F, Li H, Zhang C (2020) Assembly of GO nanosheets-coated zeolitic imidazolate framework-67 nanocubes via electrospinning and their derivatives for enhanced lithium-ion storage performance. Energy Technol 8:2000209
35. Lu Y, Hu J, Zeng Y, Zhu Y, Wang H, Lei X, Huang S, Guo L, Li L (2020) Electrochemical determination of rutin based on molecularly imprinted poly (ionic liquid) with ionic liquid-graphene as a sensitive element. Sens Actuators B 311:127911
36. Liu H, Hassan M, Bo X, Guo L (2019) Fumarate-based metal-organic framework/mesoporous carbon as a novel electrochemical sensor for the detection of gallic acid and luteolin. J Electroanal Chem 849:113378
37. Şenocak A, Khataee A, Demirbas E, Doustkhah E (2020) Ultrasensitive detection of rutin antioxidant through a magnetic micro-mesoporous graphitized carbon wrapped Co nanoarchitecture. Sens Actuators B 312:127939
38. Mohammadzadeh Jahani P, Akbari Javar H, Mahmoudi-Moghaddam H (2021) A new electrochemical sensor based on europium-doped NiO nanocomposite for detection of venlafaxine. Measurement 173:108616
39. Xie Y, Zhang T, Chen Y, Wang Y, Wang L (2020) Fabrication of core-shell magnetic covalent organic frameworks composites and their application for highly sensitive detection of luteolin. Talanta 213:120843
40. Apetrei IM, Apetrei C (2018) A modified nanostructured graphene-gold nanoparticle carbon screen-printed electrode for the sensitive voltammetric detection of rutin. Measurement 114:37–43

Authors and Affiliations

Yi Zhang[1] · Liwen Zhang[2] · Tingcui Gong[1] · Tianhao Li[2] · Xuenuan Li[2] · Jun Feng[1,2] · Tingfan Tang[2] · Hao Cheng[2,3]

[1] School of Medicine, Guangxi University of Science and Technology, Guangxi 545006 Liuzhou, People's Republic of China

[2] Guangxi Key Laboratory of Green Processing of Sugar Resources, College of Biological and Chemical Engineering, Guangxi University of Science and Technology, Guangxi 545006 Liuzhou, People's Republic of China

[3] Province and Ministry Co-sponsored Collaborative Innovation Center of Sugarcane and Sugar Industry, Guangxi 530004 Nanning, People's Republic of China